

3 Lens models

One of the main goals of lensing theory is to determine which combinations of lenses and sources can reproduce a particular image configuration. For solving this kind of problem, it is very common to use analytic lens models. These models have the advantage that they are very simple and their lensing properties can be derived quite easily.

A variety of models exists, which are more or less reliable for describing lensing on different scales. Compact objects like planets, stars, black holes or the so called Massive Astrophysical Compact Halo Objects (MACHOs) are usually well approximated by point lenses. The most simple models which are used in studies of extended lenses are the axially symmetric models. However, they are not sufficiently realistic for describing the majority of astrophysical objects, and elliptical models turn out to be much more appropriate in most cases.

3.1 Point masses

Let us begin with point masses as lenses. The deflection angle of a point mass was

$$\hat{\alpha} = -\frac{4GM}{c^2 b} \vec{e}_r, \quad (3.1)$$

where \vec{e}_r is the unit vector in radial direction. No direction is preferred in an axisymmetric situation like that, so we can identify \vec{e}_r with one coordinate axis and thus reduce the problem to one dimension. Then

$$\hat{\alpha} = \frac{4GM}{c^2 b} = \frac{4GM}{c^2 D_L \theta}, \quad (3.2)$$

where we have expressed the impact parameter by the angle θ , $b = D_L \theta$.

The lensing potential is given by

$$\hat{\Psi} = \frac{4GM}{c^2} \frac{D_{LS}}{D_L D_S} \ln |\vec{\theta}|, \quad (3.3)$$

as one can show using

$$\nabla \ln |\vec{x}| = \frac{\vec{x}}{|\vec{x}|^2}. \quad (3.4)$$

The lens equation reads

$$\beta = \theta - \frac{4GM}{c^2 D_L \theta} \frac{D_{LS}}{D_S}. \quad (3.5)$$

With the definition of the Einstein radius,

$$\theta_E \equiv \sqrt{\frac{4GM}{c^2} \frac{D_{LS}}{D_L D_S}}, \quad (3.6)$$

we have

$$\beta = \theta - \frac{\theta_E^2}{\theta}. \quad (3.7)$$

Dividing by θ_E and setting $y = \beta/\theta_E$ and $x = \theta/\theta_E$, the lens equation in its adimensional form is written as

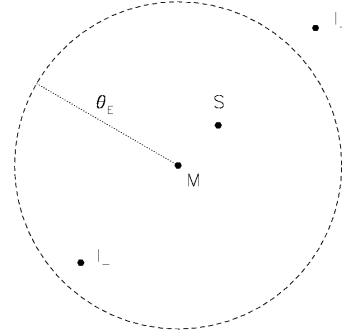
$$y = x - \frac{1}{x} \quad (3.8)$$

Multiplication with x leads to

$$x^2 - xy - 1 = 0, \quad (3.9)$$

which has two solutions:

$$x_{\pm} = \frac{1}{2} \left[y \pm \sqrt{y^2 + 4} \right]. \quad (3.10)$$



Thus, a point-mass lens has two images for any source, irrespective of its distance y from the lens. Why not three? Because its mass is singular and thus the time-delay surface is not continuously deformed.

If $y = 0$, $x_{\pm} = \pm 1$; that is, a source directly behind the point lens has a ring-shaped image with radius θ_E . For order-of-magnitude estimates:

$$\begin{aligned} \theta_E &\approx (10^{-3})'' \left(\frac{M}{M_{\odot}} \right)^{1/2} \left(\frac{D}{10 \text{kpc}} \right)^{-1/2}, \\ &\approx 1'' \left(\frac{M}{10^{12} M_{\odot}} \right)^{1/2} \left(\frac{D}{\text{Gpc}} \right)^{-1/2}, \end{aligned} \quad (3.11)$$

where

$$D \equiv \frac{D_L D_S}{D_{LS}} \quad (3.12)$$

is called *effective lensing distance*.

As $\beta \rightarrow \infty$, we see that $\theta_- = x_- \theta_E \rightarrow 0$, while obviously $\theta_+ = x_+ \theta_E \rightarrow \beta$: when the angular separation between the lens and the source becomes large, the source is unlensed. Formally, there is still an image at $\theta_- = 0$.

The magnifications follow from from the Jacobian. For any axially-symmetric lens,

$$\begin{aligned} \det A &= \frac{y}{x} \frac{\partial y}{\partial x} = \left(1 - \frac{\alpha}{x} \right) \left(1 - \frac{\partial \alpha}{\partial x} \right) \\ &= \left(1 - \frac{1}{x^2} \right) \left(1 + \frac{1}{x^2} \right) = 1 - \left(\frac{1}{x} \right)^4 \\ \Rightarrow \mu &= \left[1 - \left(\frac{1}{x} \right)^4 \right]^{-1}, \end{aligned} \quad (3.13)$$

i.e. a source at $y = 1$ has two images at

$$x_{\pm} = \frac{1 \pm \sqrt{5}}{2}, \quad (3.14)$$

and their magnifications are

$$\mu_{\pm} = \left[1 - \left(\frac{2}{1 \pm \sqrt{5}} \right)^4 \right]^{-1}. \quad (3.15)$$

For general source positions,

$$\begin{aligned} \mu_{\pm} &= \left[1 - \left(\frac{1}{x_{\pm}} \right)^4 \right]^{-1} \\ &= \frac{x_{\pm}^4}{x_{\pm}^4 - 1} = \frac{1}{2} \pm \frac{y^2 + 2}{2y\sqrt{y^2 + 4}}. \end{aligned} \quad (3.16)$$

Note that $\lim_{y \rightarrow \infty} \mu_{-} = 0$ and that $\lim_{y \rightarrow \infty} \mu_{+} = 1$: even if the lens equation has always two solutions, for large angular separations between the source and the lens, one image disappears because it is demagnified. The other is completely undistiguishable from the source because it has the same flux and the same position.

The total magnification of a point source by a point mass is thus

$$\mu = |\mu_{+}| + |\mu_{-}| = \frac{y^2 + 2}{y\sqrt{y^2 + 4}}, \quad (3.17)$$

and the magnification ratio of the two images is

$$\left| \frac{\mu_{-}}{\mu_{+}} \right| = \left(\frac{y - \sqrt{y^2 + 4}}{y + \sqrt{y^2 + 4}} \right)^2 = \left(\frac{x_{-}}{x_{+}} \right). \quad (3.18)$$

If $\beta = \theta_E$, $y = 1$ and the total magnification is $\mu = 1.17 + 0.17 = 1.34$. In terms of magnitudes, this correspond to $\Delta m = -2.5 \log \mu \sim 0.3$. The image forming at x_{+} contributes for $\sim 87\%$ of the total magnification.

Lensing by point masses on point sources will be discussed in detail in a following chapter. However, we can already answer to the question: how can lensing by a point mass be detected? Unless the lens is more massive than $10^6 M_{\odot}$ (for a source at cosmological distance), the angular separation between multiple images is too small to be resolved. However, the magnification effect will be detectable in many cases if the source is moving relative to the lens (for example, a star in the large magellanic cloud is in relative motion with respect to a star in the halo of our galaxy). Thus, since the magnification changes as a function of the angular separation between source and lens, the lensing effect will induce a time variability in the light curve of the source.

3.2 Axially symmetric lenses

The main advantage of using axially symmetric lenses is that their surface density is independent on the position angle with respect to lens center. If we choose the optical axis such that it intercepts the lens plane in the lens center, this implies that $\Sigma(\vec{\xi}) = \Sigma(|\vec{\xi}|)$. The lensing equations therefore reduce to a one-dimensional form, since all the light rays from a (point) source lie on the same plane passing through the center of the lens, the source and the observer.

The deflection angle for an axially symmetric lens was found to be

$$\hat{\alpha}(\xi) = \frac{4GM(\xi)}{c^2\xi}. \quad (3.19)$$

If want to use adimensional quantities:

$$\begin{aligned} \alpha(x) &= \frac{D_L D_{LS}}{\xi_0 D_S} \hat{\alpha}(\xi_0 x) \\ &= \frac{D_L D_{LS}}{\xi_0 D_S} \frac{4GM(\xi_0 x)}{c^2 \xi_0} \frac{\pi \xi_0}{\pi \xi_0} \\ &= \frac{M(\xi_0 x)}{\pi \xi_0^2 \Sigma_{cr}} \frac{1}{x} \equiv \frac{m(x)}{x}, \end{aligned} \quad (3.20)$$

where we have introduced the *dimensionless mass* $m(x)$. Note that

$$\alpha(x) = \frac{2}{x} \int_0^x x' \kappa(x') dx' \Rightarrow m(x) = 2 \int_0^x x' \kappa(x') dx'. \quad (3.21)$$

The lens equation (2.9) then becomes

$$y = x - \frac{m(x)}{x}. \quad (3.22)$$

Now, we derive formulas for several lensing quantities. To do that, we need to write the deflection angle as a vector. For an axially symmetric lens, the deflection angle points towards the lens center. Then,

$$\vec{\alpha}(\vec{x}) = \frac{m(\vec{x})}{x^2} \vec{x}, \quad (3.23)$$

where $\vec{x} = (x_1, x_2)$.

By differentiating we obtain:

$$\frac{\partial \alpha_1}{\partial x_1} = \frac{dm}{dx} \frac{x_1^2}{x^3} + m \frac{x_2^2 - x_1^2}{x^4}, \quad (3.24)$$

$$\frac{\partial \alpha_2}{\partial x_2} = \frac{dm}{dx} \frac{x_2^2}{x^3} + m \frac{x_1^2 - x_2^2}{x^4}, \quad (3.25)$$

$$\frac{\partial \alpha_1}{\partial x_2} = \frac{\partial \alpha_2}{\partial x_1} = \frac{dm}{dx} \frac{x_1 x_2}{x^3} - 2m \frac{x_1 x_2}{x^4}, \quad (3.26)$$

which immediately give the elements of the Jacobian matrix:

$$\begin{aligned} A &= I - \frac{m(x)}{x^4} \begin{pmatrix} x_2^2 - x_1^2 & -2x_1 x_2 \\ -2x_1 x_2 & x_1^2 - x_2^2 \end{pmatrix} \\ &\quad - \frac{dm(x)}{dx} \frac{1}{x^3} \begin{pmatrix} x_1^2 & x_1 x_2 \\ x_1 x_2 & x_2^2 \end{pmatrix}. \end{aligned} \quad (3.27)$$

This permits us to obtain the following expressions for the convergence and the shear components:

$$\kappa(x) = \frac{1}{2x} \frac{dm(x)}{dx}, \quad (3.28)$$

$$\gamma_1(x) = \frac{1}{2}(x_2^2 - x_1^2) \left(\frac{2m(x)}{x^4} - \frac{dm(x)}{dx} \frac{1}{x^3} \right), \quad (3.29)$$

$$\gamma_2(x) = x_1 x_2 \left(\frac{dm(x)}{dx} \frac{1}{x^3} - \frac{2m(x)}{x^4} \right). \quad (3.30)$$

From these relations,

$$\gamma(x) = \frac{m(x)}{x^2} - \kappa(x). \quad (3.31)$$

Since $m(x) = 2 \int_0^x x' \kappa(x') dx'$, we see that

$$\frac{m(x)}{x^2} = 2\pi \frac{\int_0^x x' \kappa(x') dx'}{\pi x^2} = \bar{\kappa}(x). \quad (3.32)$$

where $\bar{\kappa}(x) = m(x)/x^2$ is the *mean surface mass density* within x . Eq. 3.31 then reduces to

$$\gamma(x) = \bar{\kappa}(x) - \kappa(x) \quad (3.33)$$

The Jacobian determinant of the lens mapping is

$$\begin{aligned} \det A &= \frac{y}{x} \frac{dy}{dx} = \left(1 - \frac{m(x)}{x^2}\right) \left[1 - \frac{d}{dx} \left(\frac{m(x)}{x}\right)\right] \\ &= \left(1 - \frac{m(x)}{x^2}\right) \left(1 + \frac{m(x)}{x^2} - 2\kappa(x)\right) \\ &= \left(1 - \frac{\alpha(x)}{x}\right) \left(1 - \frac{d\alpha(x)}{dx}\right). \end{aligned} \quad (3.34)$$

Since the critical lines arise where $\det A = 0$, Eq. (3.34) implies that axially symmetric lenses with monotonically increasing $m(x)$ have at most two critical lines, where $m(x)/x^2 = 1$ and $d(m(x)/x)/dx = dy/dx = 1$. Both these conditions define circles on the lens plane (see Fig. 3.1). The critical line along which $m(x)/x^2 = 1$ is the tangential one: any vector which is tangential to this line is an eigenvector with zero eigenvalue of the Jacobian matrix. On the other hand, given that any vector perpendicular to the critical line where $d(m(x)/x)/dx = 1$ is also an eigenvector with zero eigenvalue, this line is the radial critical line.

From the lens equation it can be easily seen that all the points along the tangential critical line are mapped on the point $y = 0$ on the source plane. Indeed:

$$y = x \left(1 - \frac{m}{x^2}\right) = 0. \quad (3.35)$$

if x indicates a tangential critical point. Therefore, axially symmetric models have point tangential caustics. On the other hand, the points along the radial critical line are mapped onto a circular caustic on the source plane.

As discussed previously, if the lens is strong, multiple images can be formed of the same source. The number of these images depends on the position of the source with respect to the caustics. Sources which lie within the radial caustic produce three images. Sources outside the radial caustic have only one image. This is shown in Fig. 3.1. Since the tangential critical curve does not lead to a caustic curve, but the corresponding caustic degenerates to a single point $\vec{y} = 0$, the tangential critical curves have no influence on the image multiplicity. Thus, pairs of images can only be created or destroyed if the radial critical curve exists. For axially symmetric lenses, it can be shown that the necessary conditions for them to produce multiple images are (Schneider et al., 1992):

- (1) at least at one point $1 - 2\kappa(x) + \bar{\kappa}(x) < 0$: if $1 - 2\kappa(x) + \bar{\kappa}(x) > 0$ throughout, a lens produces no multiple images, since $y(x)$ increases monotonically. If on

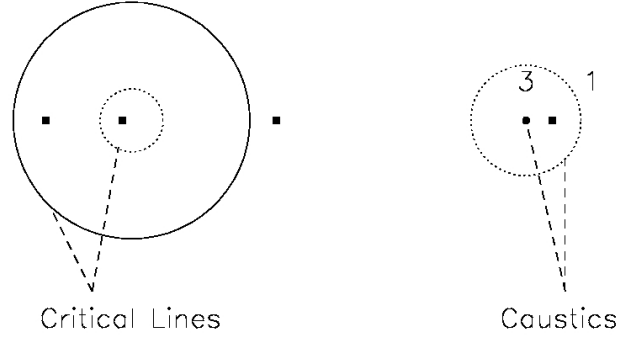


Figure 3.1: Imaging of a point source by a non-singular, circularly-symmetric lens. Left: image positions and critical lines; right: source position and corresponding caustics. From Narayan & Bartelmann (1995).

the other hand, there is a point where $dy/dx < 0$, there is at least one local maximum x_1 and one local minimum $x_2 > x_1$ of the curve $y(x)$ since $dy/dx \rightarrow 1$ for $|x| \rightarrow \infty$. For values of y such that $y(x_2) < y < y(x_1)$, there are at least three images;

- (2) $\kappa > 1/2$ at one point in the lens: if $dy/dx < 0$ at one point, then $\kappa > (1 + \bar{\kappa})/2 \geq 1/2$; a sufficient condition for multiple imaging is that $\kappa > 1$ at one point. Indeed: if κ have a a maximum at one point x_m where $\kappa(x_m) > 1$, then $\bar{\kappa}(x_m) \leq \kappa(x_m)$ and $dy/dx < 0$ at x_m . The statement then follows from (1);
- (3) if the surface density does not increase with x , $\kappa'(x) \leq 0$, $\kappa(0) > 1$: from (2) we know that it is sufficient that $\kappa > 1$ at one point for having multiple images. On the other hand if $\kappa(0) \leq 1$, then, since $y = x(1 - \bar{\kappa})$, we have for $x \geq 0$: $dy/dx = (1 - \bar{\kappa}) - x\bar{\kappa}'$. Since

$$\bar{\kappa}(x) = 2 \int_0^1 du u \kappa(ux), \quad (3.36)$$

then

$$\frac{d\bar{\kappa}}{dx} = 2 \int_0^1 du u^2 \kappa'(ux) \leq 0 \quad (3.37)$$

and $\bar{\kappa}(x) \leq \kappa(0) \leq 1$, we see that $dy/dx \geq 0$, so that no multiple images can occur.

Images are in odd numbers. A special case is that of singular lenses, i.e. lenses with infinite density at the center: in this case only two images arise when the source is within

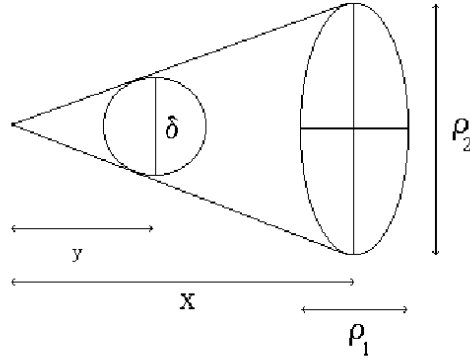


Figure 3.2: Sketch of the mapping of an infinitesimal circular source onto an elliptical image (Figure from Schneider et al., 1992).

the radial caustic. This is clear from the discussion in Sect. (2.6): when the singularity is present, the central maximum of the time delay surface is suppressed. Therefore one possible image is missed.

As was pointed out in the previous chapter, the eigenvalues of the Jacobian matrix give the inverse magnification of the image along the tangential and radial directions. Fig. (3.2) illustrates an infinitesimal source of diameter δ at position y and its image, which is an ellipse, whose minor and major axes are ρ_1 and ρ_2 respectively, at position x . With respect to the origin of the reference frame on the source plane, the circular source subtends an angle $\phi = \delta/y$. Due to the axial symmetry of the lens, $\phi = \rho_2/x$. Using the lens equation, we thus obtain

$$\frac{\delta}{\rho_2} = 1 - \frac{m(x)}{x^2}. \quad (3.38)$$

The lens mapping gives $\delta = \rho_1(dy/dx)$, from which

$$\frac{\delta}{\rho_1} = 1 + \frac{m(x)}{x^2} - 2\kappa(x) \quad (3.39)$$

This means that the image is stretched in the tangential direction by a factor $[1 - m(x)/x^2]^{-1}$ and in the radial direction by $[1 + m(x)/x^2 - 2\kappa(x)]^{-1}$.

Such distortions are more evident if the sources are extended. Fig. 3.3 shows the images of two extended sources lensed by the same model as in Fig. 3.1. One source is located close to the point-like caustic in the center of the lens. It is imaged onto the two long, tangentially oriented arcs close to the outer critical curve and the very faint image at the lens center. The other source is located on the outer caustic and forms a radially elongated image which is composed of two merging images, and a third tangentially oriented image outside the outer critical line.

3.2.1 Singular Isothermal Sphere

One of the most widely used axially symmetric model is the Singular Isothermal Sphere (SIS hereafter). The density profile of this model can be derived assuming that the

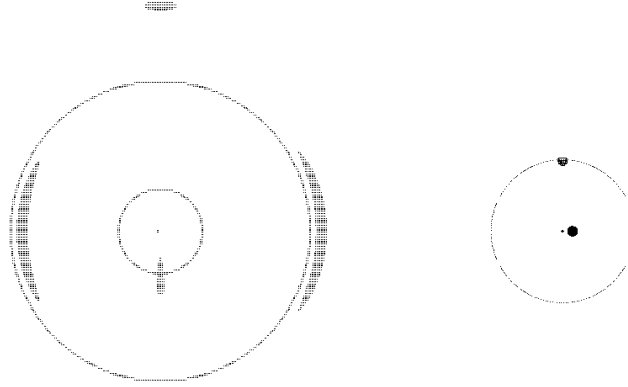


Figure 3.3: Imaging of an extended source by a non-singular circularly-symmetric lens. A source close to the point caustic at the lens center produces two tangentially oriented arc-like images close to the outer critical curve, and a faint image at the lens center. A source on the outer caustic produces a radially elongated image on the inner critical curve, and a tangentially oriented image outside the outer critical curve. From Narayan & Bartelmann (1995).

matter content of the lens behaves as an ideal gas confined by a spherically symmetric gravitational potential. This gas is taken to be in thermal and hydrostatic equilibrium. One of the two density profiles satisfying these sets of equations is given by

$$\rho(r) = \frac{\sigma_v^2}{2\pi G r^2}, \quad (3.40)$$

where σ_v is the velocity dispersion of the “gas” particles and r is the distance from the sphere center. By projecting the three-dimensional density along the line of sight, we obtain the corresponding surface density

$$\begin{aligned} \Sigma(\xi) &= 2 \frac{\sigma_v^2}{2\pi G} \int_0^\infty \frac{dz}{\xi^2 + z^2} \\ &= \frac{\sigma_v^2}{\pi G \xi} \left[\arctan \frac{z}{\xi} \right]_0^\infty \\ &= \frac{\sigma_v^2}{2G\xi}. \end{aligned} \quad (3.41)$$

This density profile has a singularity at $\xi = 0$, where the density is ideally infinite. Nevertheless, it has been used to describe the matter distribution in galaxies, especially because it can reproduce the flat rotation curves of spiral galaxies.

By choosing

$$\xi_0 = 4\pi \left(\frac{\sigma_v}{c} \right)^2 \frac{D_L D_{LS}}{D_S} \quad (3.42)$$

as the length scale on the lens plane, we obtain:

$$\Sigma(x) = \frac{\sigma_v^2 \xi_0}{2G\xi \xi_0} = \frac{1}{2x} \frac{c^2}{4\pi G} \frac{D_S}{D_L D_{LS}} = \frac{1}{2x} \Sigma_{\text{cr}} . \quad (3.43)$$

Thus, the convergence for the singular isothermal profile is

$$\kappa(x) = \frac{1}{2x} , \quad (3.44)$$

and the lensing potential (2.15) is

$$\Psi(x) = |x| . \quad (3.45)$$

Using Eqs. (2.16), we obtain

$$\alpha(x) = \frac{x}{|x|} , \quad (3.46)$$

and the lens equation reads

$$y = x - \frac{x}{|x|} . \quad (3.47)$$

If $y < 1$, two solutions of the lens equation exist. They arise at $x = y - 1$ and $x = y + 1$, on opposite sides of the lens center. The corresponding angular positions of the images are

$$\theta_{\pm} = \beta \pm \theta_E \quad (3.48)$$

where θ_E is the *Einstein radius*, defined now as

$$\theta_E = \sqrt{\frac{4GM(\theta_E)}{c^2} \frac{D_{LS}}{D_L D_S}} . \quad (3.49)$$

The quantity $M(\theta_E)$ is the mass within the Einstein radius. The angular separation between the two images therefore is $\Delta(\theta) = 2\theta_E$: the Einstein radius defines a typical scale for separation between multiple images.

On the other hand, if $y > 1$, Eq. (3.47) has a unique solution, $x = y + 1$. Images arising at $x > 0$ are of type I (positive parity), while those arising at $x < 0$ are of type II (negative parity).

The shear follows from the derivatives of Ψ . Since

$$\frac{\partial \Psi}{\partial x_i} = \frac{x_i}{|x|} \quad (3.50)$$

we have

$$\frac{\partial \Psi}{\partial x_i \partial x_j} = \frac{\delta_{ij}x - x_i x_j / x}{x^2} = \frac{\delta_{ij}x^2 - x_i x_j}{x^3} , \quad (3.51)$$

and thus

$$\Psi_{11} = \frac{x^2 - x_1^2}{x^3} = \frac{x_2^2}{x^3} \quad (3.52)$$

$$\Psi_{12} = -\frac{x_1 x_2}{x^3} \quad (3.53)$$

$$\Psi_{22} = \frac{x^2 - x_2^2}{x^3} = \frac{x_1^2}{x^3}. \quad (3.54)$$

The shear components are

$$\gamma_1 = \frac{1}{2}(\Psi_{11} - \Psi_{22}) = \frac{1}{2} \frac{x_2^2 - x_1^2}{x^3} = \frac{1}{2} \frac{\sin^2 \phi - \cos^2 \phi}{x} = -\frac{1}{2} \frac{\cos 2\phi}{x}, \quad (3.55)$$

$$\gamma_2 = \Psi_{12} = -\frac{\cos \phi \sin \phi}{x} = -\frac{1}{2} \frac{\sin 2\phi}{x}. \quad (3.56)$$

Thus,

$$\gamma(x) = (\gamma_1^2 + \gamma_2^2)^{1/2} = \frac{1}{2x} = \kappa(x). \quad (3.57)$$

From Eq. (3.47), the magnification as a function of the image position is given by

$$\mu = \frac{|x|}{|x| - 1}. \quad (3.58)$$

Images are only magnified in the tangential direction, since the radial eigenvalue of the Jacobian matrix is unity everywhere.

If $y < 1$, the magnifications of the two images are

$$\mu_+ = \frac{y+1}{y} = 1 + \frac{1}{y}; \quad \mu_- = \frac{|y-1|}{|y-1|-1} = \frac{-y+1}{-y} = 1 - \frac{1}{y}, \quad (3.59)$$

from which we see that for $y \rightarrow 1$, the second image becomes weaker and weaker until it disappears at $y = 1$. On the other hand, for $y \rightarrow \infty$, the source magnification obviously tends to unity: sources which are at large distance from the lens can only be weakly magnified by gravitational lensing.

3.2.2 Softened Isothermal Sphere

The singular isothermal sphere produces only two images of a background point source, because the time-delay surface is not continuously deformed due to the singularity in the lensing mass distribution. The singularity can be avoided by introducing a core radius, x_c , into the potential,

$$\Psi = \sqrt{x^2 + x_c^2}. \quad (3.60)$$

Then, the deflection angle is

$$\vec{\alpha}(\vec{x}) = \frac{\vec{x}}{\sqrt{x^2 + x_c^2}}, \quad (3.61)$$

and convergence and shear turn out to be

$$\kappa = \frac{x^2 + 2x_c^2}{2(x^2 + x_c^2)^{3/2}} \quad (3.62)$$

$$\gamma_1 = -\kappa \cos 2\phi \quad (3.63)$$

$$\gamma_2 = -\kappa \sin 2\phi \quad (3.64)$$

3.2.3 The Navarro-Frenk & White density profile

Navarro et al. (1997) (NFW hereafter) found that the density profile of dark matter halos numerically simulated in the framework of CDM cosmogony can be very well described by the radial function

$$\rho(r) = \frac{\rho_s}{(r/r_s)(1+r/r_s)^2}, \quad (3.65)$$

within the wide mass range $3 \times 10^{11} \lesssim M_{vir}/(h^{-1}M_\odot) \lesssim 3 \times 10^{15}$. The logarithmic slope of this density profile changes from -1 at the center to -3 at large radii. Therefore, it is flatter than that of the SIS in the inner part of the halo, and steeper in the outer part. The two parameters r_s and ρ_s are the scale radius and the characteristic density of the halo.

NFW parameterized dark matter halos by their masses M_{200} , i.e. the masses enclosed in spheres with radius r_{200} in which the average density is 200 times the critical density. The relationship between M_{200} and r_{200} is given by

$$r_{200} = 1.63 \times 10^{-2} \left(\frac{M_{200}}{h^{-1}M_\odot} \right)^{1/3} \left[\frac{\Omega_0}{\Omega(z)} \right]^{-1/3} (1+z)^{-1} h^{-1} \text{ kpc}. \quad (3.66)$$

This definition depends on the redshift z at which the halo is identified as well as on the background cosmological model.

From the former definition of r_{200} , the *concentration*, $c \equiv r_{200}/r_s$, and the characteristic density are linked by the relation,

$$\rho_s = \frac{200}{3} \rho_{cr} \frac{c^3}{[\ln(1+c) - c/(1+c)]}. \quad (3.67)$$

Numerical simulations show that the scale radii of dark matter halos at any redshift z systematically change with mass in such a way that concentration is a characteristic function of M_{200} .

Several algorithms have been suggested for describing the concentration of dark matter halos. They are all based on the assumption that the central density of a halo reflects the mean cosmic density at the time when the halo formed. This is justified by numerical simulations of structure formation, which show that halos are the more concentrated the earlier they form. Originally, NFW devised the following approach. Each halo is assigned a collapse redshift, defined as the redshift at which half of the halo mass is contained in progenitors more massive than a fraction f_{NFW} of the final mass. Then, the characteristic density is taken to be some factor C times the mean cosmic density at the collapse redshift. For fitting the results of their numerical simulations, they use $f_{\text{NFW}} = 0.01$ and $C = 3 \times 10^3$.

Bullock et al. (2001) suggested a different definition, because they noticed that the concentrations of numerically simulated dark matter halos change more rapidly with redshift than predicted by the NFW approach. They define the collapse redshift such that the non-linear mass scale at that redshift is a fraction f_B of the final halo mass. The halo concentration is then assumed to be a factor K times the ratio of the scale factors at the redshift when the halo is identified and at the collapse redshift. The best fitting values they found when comparing to numerical simulations are $f_B = 0.01$ and $K = 4$.

Finally, Eke et al. (2001) suggested another different approach. The collapse redshift of a halo of mass M is defined such that the suitably defined amplitude of the linearly evolving power spectrum at the mass scale M matches a constant C_E^{-1} . The halo concentration is then obtained by setting the characteristic density equal to the spherical

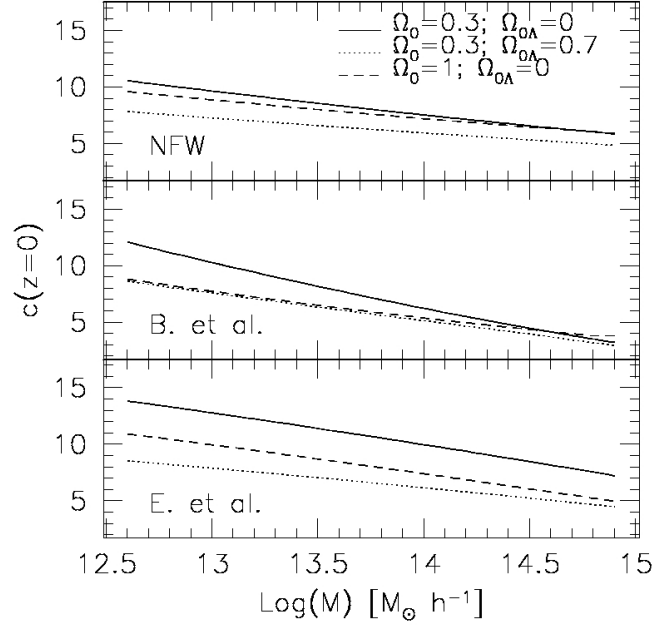


Figure 3.4: Halo concentration parameters as function of halo masses M_{200} . Results obtained for three different approaches for calculating the concentration are shown; these are the approaches by Navarro, Frenk & White (NFW; top panel), by Bullock et al. (B. et al.; middle panel) and by Eke et al. (E. et al.; bottom panel). In each panel we show the curves for a low-density OCDM model ($\Omega_0 = 0.3$, $\Omega_{0\Lambda} = 0$; solid lines), for a flat low-density Λ CDM model ($\Omega_0 = 0.3$, $\Omega_{0\Lambda} = 0.7$; dotted lines) and for a SCDM model ($\Omega_0 = 1$, $\Omega_{0\Lambda} = 0$; dashed lines).

collapse density at the collapse epoch. Numerical results are well represented assuming $C_E = 28$.

The mass-dependence of the concentration parameter c is shown in Fig. (3.4) for all the definitions of halo concentration discussed before and for different cosmological models. The main features of these plots can be summarized as follows:

- although halo concentrations produced by these different algorithms differ in detail, they have in common that the concentration increases toward lower masses in all the cosmological models considered. This is a direct result of the higher collapse redshift of less massive systems;
- the concentration depends on cosmology. The collapse redshift is determined by Ω_0 and $\Omega_{0\Lambda}$: halos form earlier in open low-density universes, then in flat low-density universes and later in flat high-density universes. The concentration thus reflects the mean cosmic density at the time when they collapse. For example, halos in an OCDM model ($\Omega_0 = 0.3$, $\Omega_{0\Lambda} = 0$) are generally more concentrated than halos in Λ CDM ($\Omega_0 = 0.3$, $\Omega_{0\Lambda} = 0.7$) or SCDM ($\Omega_0 = 1$, $\Omega_{0\Lambda} = 0$) models, because they form earlier and the mean cosmic density is higher when they collapse. On the other hand, halos formed in a low-density Λ CDM model are less concentrated than those formed in the SCDM model: even if they have a higher collapse redshift, the mean cosmic density is lower when they form.

Several different aspects of lensing by halos with NFW or generalized NFW profiles can be found in Bartelmann (1996), Wright & Brainerd (2000), Li & Ostriker (2002), Wyithe, Turner & Spergel (2001), Perrotta et al. (2002), Meneghetti et al. (2002), Bartelmann et al. (2002a,b). If we take $\xi_0 = r_s$, the density profile (3.65) implies the surface mass density

$$\Sigma(x) = \frac{2\rho_s r_s}{x^2 - 1} f(x), \quad (3.68)$$

with

$$f(x) = \begin{cases} 1 - \frac{2}{\sqrt{x^2-1}} \arctan \sqrt{\frac{x-1}{x+1}} & (x > 1) \\ 1 - \frac{2}{\sqrt{1-x^2}} \operatorname{arctanh} \sqrt{\frac{1-x}{1+x}} & (x < 1) \\ 0 & (x = 1) \end{cases}. \quad (3.69)$$

The lensing potential is given by

$$\Psi(x) = 4\kappa_s g(x), \quad (3.70)$$

where

$$g(x) = \frac{1}{2} \ln^2 \frac{x}{2} + \begin{cases} 2 \arctan^2 \sqrt{\frac{x-1}{x+1}} & (x > 1) \\ -2 \operatorname{arctanh}^2 \sqrt{\frac{1-x}{1+x}} & (x < 1) \\ 0 & (x = 1) \end{cases}, \quad (3.71)$$

and $\kappa_s \equiv \rho_s r_s \Sigma_{cr}^{-1}$. This implies the deflection angle

$$\alpha(x) = \frac{4\kappa_s}{x} h(x), \quad (3.72)$$

with

$$h(x) = \ln \frac{x}{2} + \begin{cases} \frac{2}{\sqrt{x^2-1}} \arctan \sqrt{\frac{x-1}{x+1}} & (x > 1) \\ \frac{2}{\sqrt{1-x^2}} \operatorname{arctanh} \sqrt{\frac{1-x}{1+x}} & (x < 1) \\ 1 & (x = 1) \end{cases}. \quad (3.73)$$

It is an important feature of the NFW lensing potential [Eq. (3.70)] that its radial profile is considerably less curved near the center than the SIS profile [Eq. (3.45)]. Since the local imaging properties are determined by the curvature of Ψ , this immediately implies substantial changes to the lensing properties [see Fig. (3.5)].

The convergence can be written as

$$\kappa(x) = \frac{\Sigma(\xi_0 x)}{\Sigma_{cr}} = 2\kappa_s \frac{f(x)}{x^2 - 1}, \quad (3.74)$$

from which we obtain the dimensionless mass,

$$m(x) = 2 \int_0^x \kappa(x') x' dx' = 4\kappa_s h(x). \quad (3.75)$$

The lens equation for this kind of lens model can be solved by using numerical methods. At fixed halo mass, the critical curves of an NFW lens are closer to its center than for SIS lens because of its flatter density profile. There, the potential is less curved, thus the image magnification is larger and decreases more slowly away from the critical curves. Therefore NFW lenses are less efficient in image splitting than SIS lenses, but comparably efficient in image magnification.

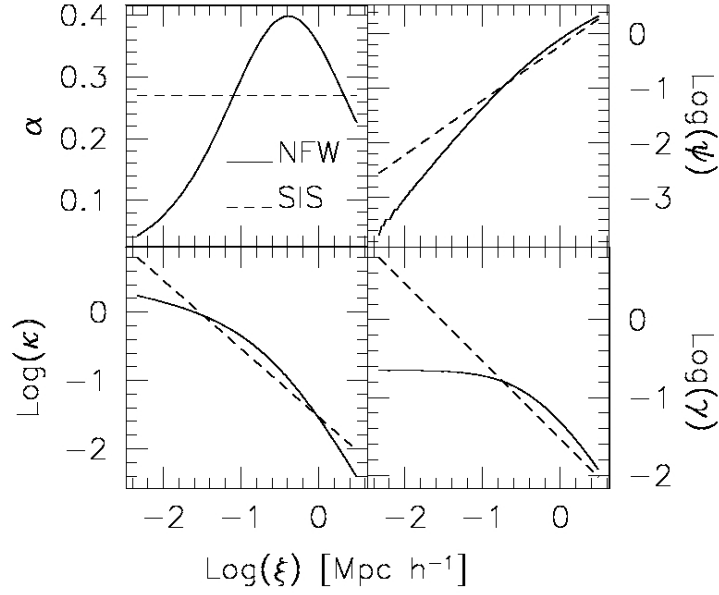


Figure 3.5: Some properties of NFW and SIS lenses as functions of the distance from the lens center. Top left panel: reduced deflection angle; top right panel: lensing potential; bottom left panel: convergence; bottom right panel: shear.

3.3 Towards more realistic lenses

3.3.1 External perturbations

It is often necessary to embed a lens into an external shear field which is created by matter in the neighbourhood. We want to represent this shear by a potential Ψ_γ , which must satisfy the following conditions:

$$\begin{aligned}
 \gamma_1 &= \frac{1}{2}(\Psi_{11} - \Psi_{22}) = \text{const.} \\
 \gamma_2 &= \Psi_{12} = \text{const.} \\
 \kappa &= \frac{1}{2}(\Psi_{11} + \Psi_{22}) = \text{const.} .
 \end{aligned} \tag{3.76}$$

If $\Psi_{11} \pm \Psi_{22}$ are required to be constant, Ψ_{11} and Ψ_{22} must separately be constants, thus

$$\Psi_\gamma = Cx_1^2 + C'x_2^2 + Dx_1x_2 + E . \tag{3.77}$$

This requires

$$\begin{aligned}\frac{1}{2}(\Psi_{11} - \Psi_{22}) &= C - C' = \gamma_1 \\ \Psi_{12} &= D = \gamma_2 \\ \frac{1}{2}(\Psi_{11} + \Psi_{22}) &= C + C' = \kappa\end{aligned}\tag{3.78}$$

Imposing $\kappa = 0$, we obtain

$$C = C' \Rightarrow C = \frac{\gamma_1}{2}.\tag{3.79}$$

Therefore,

$$\Psi_\gamma = \frac{\gamma_1}{2}(x_1^2 - x_2^2) + \gamma_2 x_1 x_2\tag{3.80}$$

Likewise, if we want to place our lens on a sheet of constant surface-mass density, the shear of that sheet must be zero (because no direction can be preferred), and from Eq. 3.78 we find

$$\Psi_\kappa = \frac{\kappa}{2}(x_1^2 + x_2^2).\tag{3.81}$$

Irrelevant constants have been suppressed above.

We can now embed e.g. a softened isothermal sphere into a constant shear field,

$$\Psi = \sqrt{x^2 + x_c^2} + \frac{\gamma_1}{2}(x_1^2 - x_2^2) + \gamma_2 x_1 x_2\tag{3.82}$$

yielding the deflection angle

$$\begin{aligned}\vec{\nabla}\Psi &= \frac{\vec{x}}{\sqrt{x^2 + x_c^2}} + \begin{pmatrix} \gamma_1 x_1 + \gamma_2 x_2 \\ -\gamma_1 x_2 + \gamma_2 x_1 \end{pmatrix} \\ &= \frac{\vec{x}}{\sqrt{x^2 + x_c^2}} + \begin{pmatrix} \gamma_1 & \gamma_2 \\ \gamma_2 & -\gamma_1 \end{pmatrix} \vec{x}\end{aligned}\tag{3.83}$$

and the convergence remains unchanged by construction.

The deflection angle of a sheet of constant surface-mass density is

$$\vec{\alpha} = \vec{\nabla}\Psi_\kappa = \kappa \vec{x}.\tag{3.84}$$

Thus, the lens equation reads, in this case,

$$\vec{y} = \vec{x} - \vec{\alpha} = \vec{x}(1 - \kappa).\tag{3.85}$$

If $\kappa = 1$, $y = 0$ for all images, i.e. this sheet focuses all light rays exactly on the origin. This gravitational lens thus has a well-defined focal point.

Remark:

When combining the potentials of the lens and of external perturbers the same scale ξ_0 must be chosen if using adimensional coordinates.

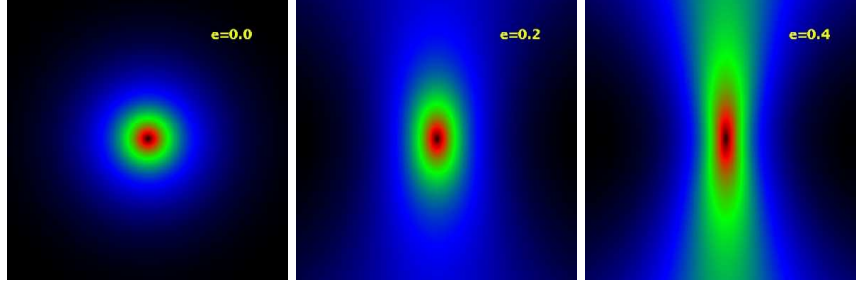


Figure 3.6: Deflection angle map for an axially symmetric (left panel) and elliptically distorted NFW lens model, for ellipticity 0.2 (central panel) and 0.4 (right panel). The lens mass and redshift are $10^{15}M_{\odot}h^{-1}$ and 0.3 respectively. The source redshift is 1. The side length of each panel is $\sim 6'$.

3.3.2 Elliptical lenses

A circularly symmetric lens model is too much idealized to describe the properties of real lenses, like galaxies or galaxy clusters. Slightly less unrealistic models are obtained by adding two more parameters: the ellipticity and the position angle describing the orientation of the lens.

The construction of lens models with elliptical or pseudo-elliptical isodensity contours is generally quite complicated Kassiola et al. (1992); Kormann et al. (1994); Golse & Kneib (2002). One can start from the projected surface-mass density of an axially symmetric model

$$\Sigma(x) = f(x) \quad (3.86)$$

and can obtain its elliptical generalization by substituting

$$x \rightarrow X = \sqrt{\frac{x_1^2}{(1-e)} + x_2^2(1-e)}, \quad (3.87)$$

where $e = 1 - b/a$ is the ellipticity and a and b are the major and minor axis of the ellipse. This ensures that the mass inside circles of fixed radius remains constant as the ellipticity changes. The resulting model will have elliptical iso-density contours whose major axis will be oriented along the x_2 -direction. The model can then arbitrarily rotated by the desired position angle, θ .

The complication in this approach comes from the fact that obtaining the potential corresponding to these kinds of density distributions can become extremely complicated, even for quite simple lens models. It is simpler and often sufficient to model a lens by means of an elliptical effective lensing potential.

For any axially symmetric lensing potential in the form

$$\Psi(x) = g(x) \quad (3.88)$$

the same substitution given in Eq. 3.87 can be carried out.

The Cartesian components of the deflection angle are then

$$\begin{aligned} \alpha_1 &= \frac{\partial \Psi}{\partial x_1} = \frac{x_1}{(1-e)X} \tilde{\alpha}(X), \\ \alpha_2 &= \frac{\partial \Psi}{\partial x_2} = \frac{x_2(1-e)}{X} \tilde{\alpha}(X), \end{aligned} \quad (3.89)$$

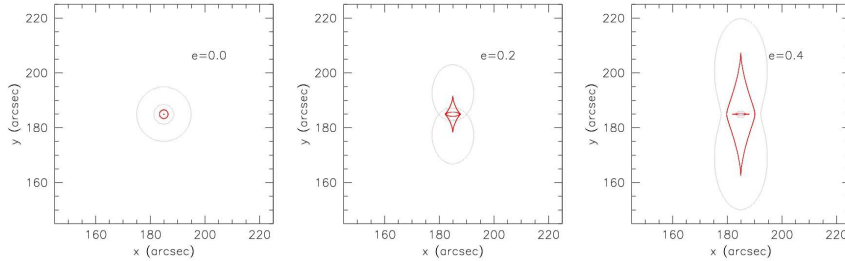


Figure 3.7: Critical lines (black lines) and caustics (red lines) for the same lens models as in Fig. (3.6).

where $\tilde{\alpha}(X)$ is the unperturbed (i.e. axially-symmetric) deflection angle at the distance X from the lens center.

Using these formulae, deflection-angle fields for different values of the ellipticity e are readily computed. Some examples for deflection-angle maps are displayed in Fig. (3.6), where ellipticity is included in the lensing potential of the sphere with the NFW density profile. Starting from an elliptical lensing potential is computationally much more tractable, but has the disadvantage that the deflection angle field and the mass distribution corresponding to the elliptical potential can become dumbbell-shaped even for moderate ellipticities. This is unwanted for galaxy lenses but admissible for galaxy clusters, because they are less relaxed and exhibit substructure.

Increasing the ellipticity of the lensing potential strengthens the shear field of the lens, and consequently the caustics and the critical lines expand and change. Examples for the change of the caustics and of the critical lines with ellipticity e for a pseudo-elliptical NFW halo are shown in Fig. (3.7), which refers to a lens with mass $M = 10^{15} h^{-1} M_{\odot}$ at redshift $z = 0.3$, and the underlying cosmology is the Λ CDM model. As discussed above, the radial and tangential caustics are a circle and a point, respectively, for the axially symmetric models. Increasing e , the caustics stretch, develop cusps, and enclose an increasing area. The critical lines, which are originally circles on the lens plane, are stretched as well and assume the dumbbell shape which characterizes the surface density distribution of the lens.

In the case of non-axially symmetric lenses, a wide variety of image configurations can be produced. Some examples are shown in Fig. (3.8). Compared to the axially-symmetric case, when the source is enclosed within two caustics, it has five images. One appears at the lens center, and the four others form a cross-shaped pattern. When the source is moved outward, two of the four outer images move along the tangential critical line towards each other, merge, and disappear when the source crosses the tangential caustic. Three images remain until the source crosses the radial caustic, when two more images approach each other perpendicular to the radial critical line, merge and disappear. After that, only one weakly distorted image remains.

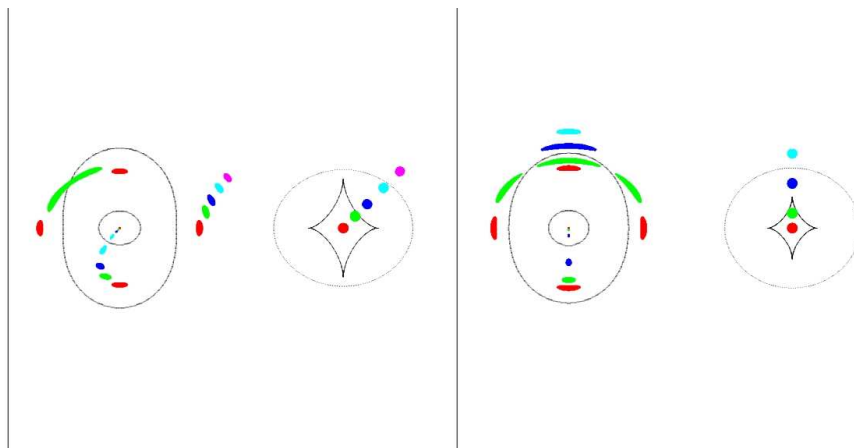


Figure 3.8: Compact source moving away from the center of an elliptical lens. Left panel: source crossing a fold caustic; right panel: source crossing a cusp caustic. Within each panel the digram on the right shows the caustics and the source positions and the left diagram shows the critical lines and the corresponding image positions (Figure from Narayan & Bartelmann, 1995).